Eur. Phys. J. D **38**, 175–184 (2006)
DOI: 10.1140/epjd/e2005-00332-1

THE EUROPEAN PHYSICAL JOURNAL D

Orientation of Cs $6p\,^2P_{3/2}$ atomic photofragments in a magnetic field: interference in the photodissociation of diatomic molecules

Y. Kimura[a]

Tsukuba Magnet Laboratory, National Institute for Materials Science, 3-13 Sakura, Tsukuba, 305-0003 Japan

Received 19 July 2005
Published online 20 December 2005

Abstract. In a magnetic field, Cs_2 molecules were excited from the ground $X\,^1\Sigma_g^+(v_X = 0, J_X = 55)$ level to the $D\,^1\Sigma_u^+(v = 46, J = 54)$ level by dissociation laser light linearly polarized parallel to the field, for which the magnetic sublevels were degenerated and thus all the transitions between them were simultaneously stimulated. Probe laser light excited the dissociated Cs $6p\,^2P_{3/2}$ atomic fragments to $6p\,^2D_{3/2}$ level and the resultant $6p\,^2P_{1/2} - 6d\,^2D_{3/2}$ emission was detected as the function of the wavelength of the probe light. The populations of the $6p\,^2P_{3/2,m_j}$ magnetic sublevels were determined from the relative strengths of the $6p\,^2P_{3/2,m_j} - 6d\,^2D_{3/2,m'_j}$ transitions induced by the probe light. Non-zero orientation O_0 was found in the ensemble of dissociated Cs $6p\,^2P_{3/2}$ atomic fragments. The orientation O_0 increased as the magnetic field strength increased. It was demonstrated both experimentally and theoretically that the orientation O_0 was induced through the interference in the excitation and dissociation paths in the presence of an external magnetic field, even when all degenerated transitions between the magnetic sublevels of the molecules are simultaneously excited by the light linearly polarized parallel to the field.

PACS. 33.80.Gj Diffuse spectra; predissociation, photodissociation – 33.55.Be Zeeman and Stark effects – 42.25.Hz Interference

1 Introduction

Population distribution among the magnetic sublevels of the photodissociated fragments is governed by the dissociation dynamics [1,2]. The allowed population distribution is limited by the symmetry of the system, which consists of parent molecules, dissociation light, and sometimes the external field. For example, when molecules are excited by linearly polarized light, they can be aligned, and when excited by circularly polarized light, they can be oriented [3–5]. By a semiclassical treatment, Dixon presented a general theory for the multipole moments of the angular momentum carried by the photodissociated fragments [6]. Siebbeles et al. presented full quantum mechanical treatment [7]. A number of experiments have been reported, but most of them were limited in the case where the polarized angular momentum — alignment or orientation — was carried by dissociated molecules in their nuclear rotations [8–10]. A few experiments were reported where the alignment was carried by dissociated atoms in their electronic orbital motion following to the photodissociation by the linearly or circularly polarized light [11,12], or the orientation was carried by them following to the photodissociation by the circularly polarized light [13–15]. It should be noted that all the angular momentum polarized states observed in these experiments were the ones allowed by the restriction from the symmetry. Recently, it was observed that the atomic fragments following to the photodissociation by linearly polarized light were oriented and the orientation was explained to be generated by the quantum mechanical interference between the vibrational wavefunctions during the dissociation process [16].

Figure 1 shows potential energy curves of lower excited states of Cs_2 molecules [17–20]. The molecules in the $D\,^1\Sigma_u^+$ state were found to selectively dissociate into the separated Cs $6p\,^2P_{3/2}$+ Cs $6s\,^2S_{1/2}$ atomic fragments, and this dissociation channel was far stronger than other energetically allowed channels; Cs $6s\,^2S_{1/2}$+ Cs $6s\,^2S_{1/2}$ fragments or Cs $6p\,^2P_{1/2}$+ Cs $6s\,^2S_{1/2}$ fragments [18,21,22]. Matsubara et al. excited Cs_2 molecules from the ground $X\,^1\Sigma_g^+(v_X = 0, J_X = 55)$ level to the $D\,^1\Sigma_u^+(v = 46, J = 54)$ level in the magnetic field of 0.19 T by laser light linearly polarized parallel to the field, where $v(v_X)$ was the vibrational quantum number and $J(J_X)$ the quantum number associated with the total angular momentum $\boldsymbol{J}$ of a molecule excluding nuclear spin. The populations of the $6p\,^2P_{3/2,m_j}$ magnetic sublevels of dissociated atomic fragments were determined from the relative strengths of the $6p\,^2P_{3/2,m_j} - 8s\,^2S_{1/2,m'_j}$ transition lines induced by another laser light, where m_j was the quantum number associated with the projection to the direction of the magnetic

[a] e-mail: kimura.yasuyuki@nims.go.jp

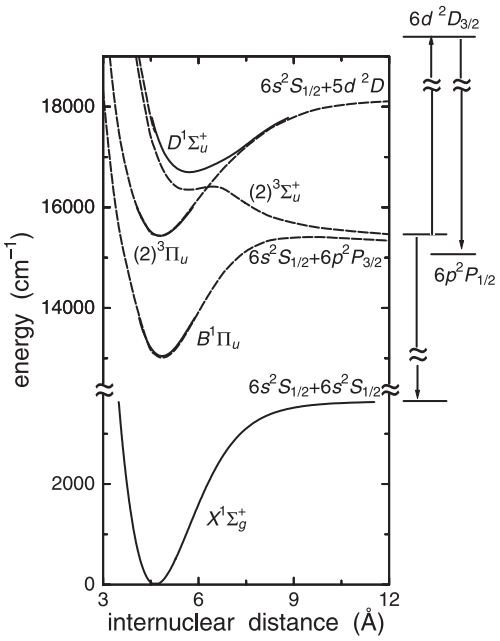

Fig. 1. Potential energy curves of the Cs_2 molecules. The RKR potential energy curves of the $D\,^1\Sigma_u^+$ and the $(2)^3\Pi_u$ states from reference [17], $X\,^1\Sigma_g^+$ from reference [18], $B\,^1\Pi_u$ from reference [19] are shown by solid curves. The curves obtained by ab initio MO calculations in reference [20] are shown by broken curves.

field (space-fixed Z-axis) of the total angular momentum $\boldsymbol{j}$ (the quantum number is j) excluding nuclear spin of a Cs atom. Non-zero orientation of the Cs $6p\,^2P_{3/2}$ atomic fragments was observed, though the parent molecules were excited by the linearly polarized light, and it could not be explained by assuming that the atoms were produced by the predissociation of the Cs_2 $D\,^1\Sigma_u^+(v = 46,\ J = 54)$ molecules through the dissociative $(2)^3\Sigma_u^+$ state [24].

Recently it was verified that the optical transition to the $(2)^3\Sigma_u^+$ state from the ground $X\,^1\Sigma_g^+$ state was allowed by the spin-orbit coupling of the $(2)^3\Sigma_u^+$ state with the $B\,^1\Pi_u$ state [25]. The probability of producing Cs $6p\,^2P_{3/2,m_j}$ atomic fragments needs to be re-evaluated by taking account of the effects of the quantum mechanical interference from this transition.

In the present report, the same $X\,^1\Sigma_g^+(v_X = 0, J_X = 55) - D\,^1\Sigma_u^+(v = 46,\ J = 54)$ transition of Cs_2 molecules prepared in a molecular beam was excited in the magnetic field, and the populations of the dissociated Cs $6p\,^2P_{3/2,m_j}$ atomic fragments were determined from the relative strengths of the laser-induced transitions to the $6d\,^2D_{3/2,m'_j}$ sublevels instead of that to the $8s\,^2S_{1/2,m'_j}$ sublevels, because the energy splittings between the neighboring transition lines of the hyperfine components in the $6p\,^2P_{3/2} - 6d\,^2D_{3/2}$ transition were smaller than those of the $6p\,^2P_{3/2} - 8s\,^2S_{1/2}$ transition and therefore the relative strength of the transition line could be evaluated clearly. The conditions of the molecular beam and the power of the laser light were controlled carefully so that the self-absorption in the $6s\,^2S_{1/2} - 6p\,^2P_{3/2}$ transition which has prevented the precise determination of the populations in the previous experiment [24], was reduced to be negligible. Since the dependence on the magnetic field strength of the population distribution of the dissociated atomic fragments would act as another probe to determine the dissociation dynamics, the populations were determined as the function of the field strength. These improvements both in the theoretical and experimental sides provided clear and novel understandings of the generation of the orientation of the dissociated atomic fragments, the mechanism of which was essentially different from the previous one proposed by Rakitzis et al. [16].

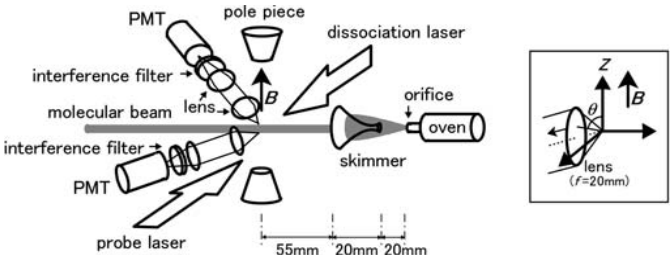

Fig. 2. Experimental set-up. The dissociation light is linearly polarized parallel to the magnetic field (Z-axis) and the probe light is perpendicular to it. Two sets of optical equipments are in the plane containing the molecular beam and the laser light. The inset shows the geometry about the objective lens and the emission from the intersection. The origin of the coordinate is chosen at the intersection.

2 Instrument and method

Figure 2 schematically shows the experimental set-up. In a vacuum chamber ($\sim 10^{-6}$ Torr), the magnetic field was applied by an electric magnet with a pair of pole pieces which was tapered to ϕ 15 mm on the tip and was inserted in the chamber. The distance between the tips was 10 mm. In the chamber, cesium metal of the purity 99.98% was kept in a stainless oven and heated to 600 K. The cesium vapor was spouted through an orifice (diameter ϕ 300 μm), collimated by a conical skimmer (ϕ 770 μm) placed 20 mm downstream from the orifice, and had the shape of beam (molecular beam). The molecular beam crossed at right angles to the magnetic field. The distance from the skimmer to the intersection of the molecular beam with the center axis of the magnetic field, was 55 mm.

Dissociation light (17466 cm^{-1}, 2.0 W/cm^2) from a single-mode tunable dye laser (Coherent 699-29, linewidth 500 kHz, R6G dye) was introduced into the chamber through a quartz window and crossed at right angles to both the magnetic field and the molecular beam. The light was linearly polarized parallel to the magnetic field. It excited the Cs_2 molecules from the ground $X\,^1\Sigma_g^+(v_X = 0,\ J_X = 55)$ level to the $D\,^1\Sigma_u^+(v = 46,\ J = 54)$ level. The resultant emission from the intersection was collected and made parallel by an objective lens (ϕ 7 mm, focal length f = 20 mm) placed in a plane containing the molecular beam and the laser light. The solid angle of the

emission-collection was 0.096 sr. The collected emission went through a quartz window on the chamber wall, a second lens (ϕ 26 mm, $f = 140$ mm), and an interference filter (transmission maximum at $\lambda_0 = 853.0$ nm, full width at half maximum FWHM = 9.0 nm). Here, the $6s\,^2\mathrm{S}_{1/2} - 6p\,^2\mathrm{P}_{3/2}$ emission (D_2-line, 852 nm) from the dissociated Cs atomic fragments was selected and was focused to a cooled photomultiplier tube (RCA C31034). The photoelectron pulses were counted by a photon counter (EG & G Princeton Applied Research Model 1109).

A probe light (10856 cm^{-1}, 1.4 $\mathrm{W/cm}^2$) from a single-mode tunable Ti:sapphire laser (Coherent 899-29, line width 500 kHz) propagated antiparallel to the dissociation light and passed the intersection. The probe light was linearly polarized perpendicular to the magnetic field. It excited the dissociated Cs $6p\,^2\mathrm{P}_{3/2}$ atoms to the $6d\,^2\mathrm{D}_{3/2}$ level. The resultant $6p\,^2\mathrm{P}_{1/2} - 6d\,^2\mathrm{D}_{3/2}$ emission (876 nm) was detected by another set of optical equipments including an interference filter ($\lambda_0 = 878.9$ nm, FWHM = 14.8 nm) and a cooled photomultiplier tube (Hamamatsu R943-02). Optical transitions concerned were also summarized in Figure 1. A small portion of the probe laser light was divided and introduced into a temperature-stabilized confocal ethalon (Burleigh CFT-500) for frequency-marks and into a photo diode detector for power-monitoring.

The photon counts of the $6p\,^2\mathrm{P}_{1/2} - 6d\,^2\mathrm{D}_{3/2}$ emission were measured as the function of the wavelength of the probe light, simultaneously with the frequency-marks, the power of the probe light and the photon counts of the $6s\,^2\mathrm{S}_{1/2} - 6p\,^2\mathrm{P}_{3/2}$ emission. The last two were used to normalize the photon counts of the the $6p\,^2\mathrm{P}_{1/2} - 6d\,^2\mathrm{D}_{3/2}$ emission against the fluctuation of both the power of the two lasers and the density of the molecular beam.

3 Results and discussions

Figure 3a shows the measured photon counts for the field strength of 0.38 (T). The nuclear spin of ^{133}Cs atom is 7/2. The hyperfine constants A of the $6d\,^2\mathrm{D}_{3/2}$ and $6p\,^2\mathrm{P}_{3/2}$ levels were reported to be 16.30 and 50.34 MHz, respectively [26]. In the magnetic field $\boldsymbol{B}$ ($B = |\boldsymbol{B}|$), nonzero matrix elements of the Hamiltonian of the hyperfine structure H_{hfs} and the Zeeman Hamiltonian $H_B^{(\mathrm{A})} = -\boldsymbol{m}_{\mathrm{A}} \cdot \boldsymbol{B}$, for the basis functions of $|6p\,^2\mathrm{P}_{3/2} f m_f\rangle$ and $|6d\,^2\mathrm{D}_{3/2} f m_f\rangle$, were given in reference [24], where $\boldsymbol{m}_{\mathrm{A}}$ is a magnetic moment of the Cs atom given by $\boldsymbol{m}_{\mathrm{A}} = -\mu_{\mathrm{B}}(\boldsymbol{l} + 2\boldsymbol{s})/\hbar$, f is a quantum number associated with the total angular momentum $\boldsymbol{f} = \boldsymbol{j} + \boldsymbol{i} = \boldsymbol{l} + \boldsymbol{s} + \boldsymbol{i}$ and m_f is the quantum number associated with the projection of $\boldsymbol{f}$ to the the Z-axis. Here, μ_{B} is the Bohr magneton, $\boldsymbol{l}$, $\boldsymbol{s}$, $\boldsymbol{j}$, $\boldsymbol{i}$ are the orbital, the spin, the total electronic and the nuclear spin angular momentum of the Cs atom, respectively. For the $6p\,^2\mathrm{P}_{3/2}$ and $6d\,^2\mathrm{D}_{3/2}$ levels respectively, the eigenvalues and eigenfunctions of the Hamiltonian $H_{\mathrm{hfs}} + H_B^{(\mathrm{A})}$ were calculated for $B = 0.38$ T. Energies and strengths of allowed transitions induced by the probe light linearly polarized perpendicular to the field, were calculated under the assumption of equal population on every $6p\,^2\mathrm{P}_{3/2}$ hyperfine sublevel. The result is shown in Figure 3b.

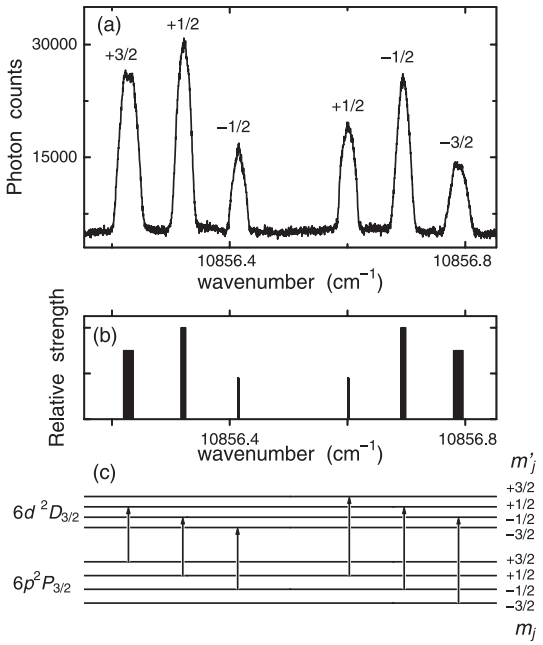

Fig. 3. (a) Observed photon counts of the $6p\,^2\mathrm{P}_{1/2} - 6d\,^2\mathrm{D}_{3/2}$ emission following to the $6p\,^2\mathrm{P}_{3/2} - 6d\,^2\mathrm{D}_{3/2}$ transition induced by the probe laser light, for the field strength of 0.38 T. The abscissa is the wavenumber of the probe light. The quantum numbers m_j denoting the $6p\,^2\mathrm{P}_{3/2,m_j}$ sublevels, are shown above the line. (b) Calculated relative strength and energy of the $6p\,^2\mathrm{P}_{3/2} - 6d\,^2\mathrm{D}_{3/2}$ transition detected at $\theta = 90^\circ$ by the $6p\,^2\mathrm{P}_{1/2} - 6d\,^2\mathrm{D}_{3/2}$ emission for the field strength of 0.38 T, where statistical distributions on the populations of the Cs $6p\,^2\mathrm{P}_{3/2}$ hyperfine sublevels is assumed. Each of the $6p\,^2\mathrm{P}_{3/2,m_j}$ and $6d\,^2\mathrm{D}_{3/2,m'_j}$ sublevels split into 8 hyperfine sublevels. Each $6p\,^2\mathrm{P}_{3/2,m_j} - 6d\,^2\mathrm{D}_{3/2,m'_j}$ transition consists of 8 hyperfine components. (c) Allowed transitions by the probe laser light linearly polarized perpendicular to the magnetic field, are shown by vertical arrows.

It was understood that for 0.38 T both the $6p^2\mathrm{P}_{3/2}$ and $6d\ ^2\mathrm{D}_{3/2}$ atoms were in the Paschen-Back region for the hyperfine interaction and thus the $6p\,^2\mathrm{P}_{3/2} - 6d\,^2\mathrm{D}_{3/2}$ transitions were grouped to six transitions classified by j and m_j. The lower and upper magnetic sublevels of the transitions are shown in Figure 3c and Table 1. The ratio of the transition probabilities between the grouped six $6p\,^2\mathrm{P}_{1/2} - 6d\,^2\mathrm{D}_{3/2}$ transitions was coincident with the ratio 3:4:3:3:4:3 from lower to higher transition energy, which was the ratio in the absence of hyperfine interaction [27]. Hereafter, the hyperfine interaction should be neglected for $B \geq 0.38$ T. The allowed transitions by the probe light ($m_j - m'_j = \pm 1$), are shown by vertical arrows in Figure 3c.

The relative strength of the $6p\,^2\mathrm{P}_{1/2,m''_j} - 6d\,^2\mathrm{D}_{3/2,m'_j}$ transition line allowed for $m''_j = m'_j, m'_j \pm 1$, observed from the direction defined by the polar angle θ from Z-axis (see

Table 1. The relative strengths I_{m_j} or I'_{m_j} of the $6p\,^2\mathrm{P}_{3/2,m_j} - 6d\,^2\mathrm{D}_{3/2,m'_j}$ transitions excited by the light linearly polarized perpendicular to the field and detected by the m_j-unresolved $6p\,^2\mathrm{P}_{1/2} - 6d\,^2\mathrm{D}_{3/2}$ emission from the direction of the polar angle θ, where I_0 is a common constant. Here, I_{m_j} is the strength through the $6d\,^2\mathrm{D}_{3/2,\pm1/2}$ sublevels and I'_{m_j} is the one through the $6d\,^2\mathrm{D}_{3/2,\pm3/2}$ sublevels. The populations σ_{m_j} can be determined from the ratio of the four I_{m_j}'s without depending on the solid angle of the detection of the $6p\,^2\mathrm{P}_{1/2} - 6d\,^2\mathrm{D}_{3/2}$ emission.

$6p\,^2\mathrm{P}_{3/2}$	$6d\,^2\mathrm{D}_{3/2}$	relative strength I_{m_j}, I'_{m_j}
$+3/2$	$+1/2$	$I_{+3/2} = \sigma_{+3/2} 3(4\sin^2\theta + \cos^2\theta + 1) I_0$
$+1/2$	$-1/2$	$I_{+1/2} = \sigma_{+1/2} 4(4\sin^2\theta + \cos^2\theta + 1) I_0$
$-1/2$	$-3/2$	$I'_{-1/2} = \sigma_{-1/2} 3(3\cos^2\theta + 3) I_0$
$+1/2$	$+3/2$	$I'_{+1/2} = \sigma_{+1/2} 3(3\cos^2\theta + 3) I_0$
$-1/2$	$+1/2$	$I_{-1/2} = \sigma_{-1/2} 4(4\sin^2\theta + \cos^2\theta + 1) I_0$
$-3/2$	$-1/2$	$I_{-3/2} = \sigma_{-3/2} 3(4\sin^2\theta + \cos^2\theta + 1) I_0$

the inset in Fig. 2) were given by [27,28],

$$(3/2 + m'_j)(3/2 - m'_j)\sin^2\theta \qquad (6p\,^2\mathrm{P}_{1/2,m'_j} - 6d\,^2\mathrm{D}_{3/2,m'_j}), \quad (1)$$

$$\frac{1}{4}(1/2 \mp m'_j)(3/2 \mp m'_j)(1 + \cos^2\theta) \qquad (6p\,^2\mathrm{P}_{1/2,m'_j \pm 1} - 6d\,^2\mathrm{D}_{3/2,m'_j}). \quad (2)$$

The angular distributions were the well-known $\sin^2\theta$-distribution for the π-radiation and the $(1 + \cos^2\theta)/2$-distribution for the σ-radiation, respectively.

When the populations of the $6p\,^2\mathrm{P}_{3/2,m_j}$ sublevels were represented by σ_{m_j}, the strengths of the $6p\,^2\mathrm{P}_{3/2,m_j} - 6d\,^2\mathrm{D}_{3/2,m'_j}$ transitions excited by the light linearly polarized perpendicular to the field and detected by the m_j-unresolved $6p\,^2\mathrm{P}_{1/2} - 6d\,^2\mathrm{D}_{3/2}$ emission from the direction of the polar angle θ, are listed in Table 1, where I_{m_j} is the strength through the $6d\,^2\mathrm{D}_{3/2,\pm1/2}$ sublevels, I'_{m_j} through the $6d\,^2\mathrm{D}_{3/2,\pm3/2}$ sublevels, and the I_0 is a common constant. Note that the θ dependent parts of the four I_{m_j} were generated from superpositions of the angular distributions of the π- and σ-radiation of the $6p\,^2\mathrm{P}_{1/2} - 6d\,^2\mathrm{D}_{3/2,\pm1/2}$ transition in common weights and thus they were identical. Therefore, even though the m_j -unresolved $6p\,^2\mathrm{P}_{1/2} - 6d\,^2\mathrm{D}_{3/2}$ emission was collected by the objective lens, the populations σ_{m_j} of the four $6p\,^2\mathrm{P}_{3/2,m_j}$ sublevels could be determined from the ratio of the I_{m_j} without depending on the solid angle of the detection of the emission. It is understood from the comparison of Figure 3a with 3b, that the shape of the transition line was determined by the Doppler profile due to the fragment velocity obtained from the excess energy in the dissociation process, but also determined by the energy splitting of the hyperfine components. In the present, the strength of the line integrated over the whole line profile was utilized for I_{m_j} and the populations σ_{m_j} were determined, which means that the σ_{m_j} represents the populations averaged over all the fragments dissociating towards every directions (solid angle of 4π).

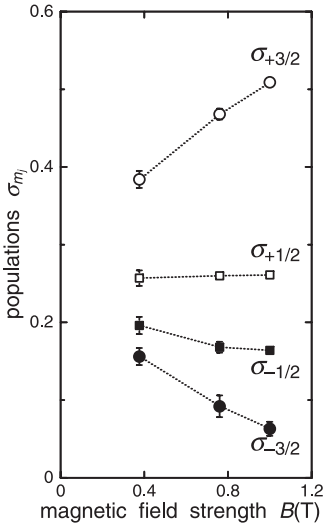

Fig. 4. The populations σ_{m_j} of the $6p\,^2\mathrm{P}_{3/2,m_j}$ sublevels as the function of the field strength B. The uncertainties are estimated from the standard deviations of the values determined by the measurements which are repeated five times.

The procedure of the measurement was repeated five times. The averaged values of the populations σ_{m_j} were shown in Figure 4, where σ_{m_j} were normalized to unity. The uncertainties were estimated from the standard deviations of the values determined by the measurements repeated five times. The procedure was repeated by changing the relative power of the probe light against the dissociation light. The obtained σ_{m_j} were confirmed to be free from the saturation in the optical transition. Similar procedures were repeated for 0.76 T and 1.00 T. The results were also shown in Figure 4. The non-zero orientation O_0,

$$O_0 = \sum_{m_j} (2m_j/\sqrt{15})\sigma_{m_j}, \quad (3)$$

was observed in the ensemble of the dissociated Cs $6p\,^2\mathrm{P}_{3/2}$ atomic fragments. It meant that the ensemble had a net angular momentum $\langle j_Z \rangle$ along the space-fixed Z-axis. This was remarkable because the parent molecules were excited by the linearly polarized light. The orientation O_0 increased as the magnetic field strength increased.

Figure 5 schematically shows the levels related to the excitation and the dissociation with couplings between them. It has been explained that the $\mathrm{D}\,^1\Sigma_u^+(v, J, M)$ level couples with the $(2)^3\Pi_{0u}\mathrm{e}(v_P, J, M)$ level by the spin-orbit coupling H_{SO}, the $(2)^3\Pi_{0u}\mathrm{e}(v_P, J, M)$ level with the dissociative $(2)^3\Sigma_u^+(E_S, N, J, M)$ continuum by the L-uncoupling $H_{JL} = -B_{\mathrm{R}}(J_+L_- + J_-L_+)$ and then the molecules predissociate into Cs $6p\,^2\mathrm{P}_{3/2}$+ Cs $6s\,^2\mathrm{S}_{1/2}$ atomic fragments (path-α) [23,24], where v, v_P are the vibrational quantum numbers, E_S is the energy of the $(2)^3\Sigma_u^+(E_S, N, J, M)$ continuum, "e" expresses a level of parity $+(-)^J$ of the $(2)^3\Pi_{0u}\mathrm{e}(v_P, J, M)$ level, and M is the quantum number associated with the projection of $\boldsymbol{J}$ on the Z-axis. The quantum number N is associated with $\boldsymbol{J} - \boldsymbol{S}$, where $\boldsymbol{S}$ is the electronic spin angular momentum. Symbol B_{R} is the rotational constant, $J_\pm$,$L_\pm$ are the raising and lowering operators associated with $\boldsymbol{J}$ or $\boldsymbol{L}$ on the

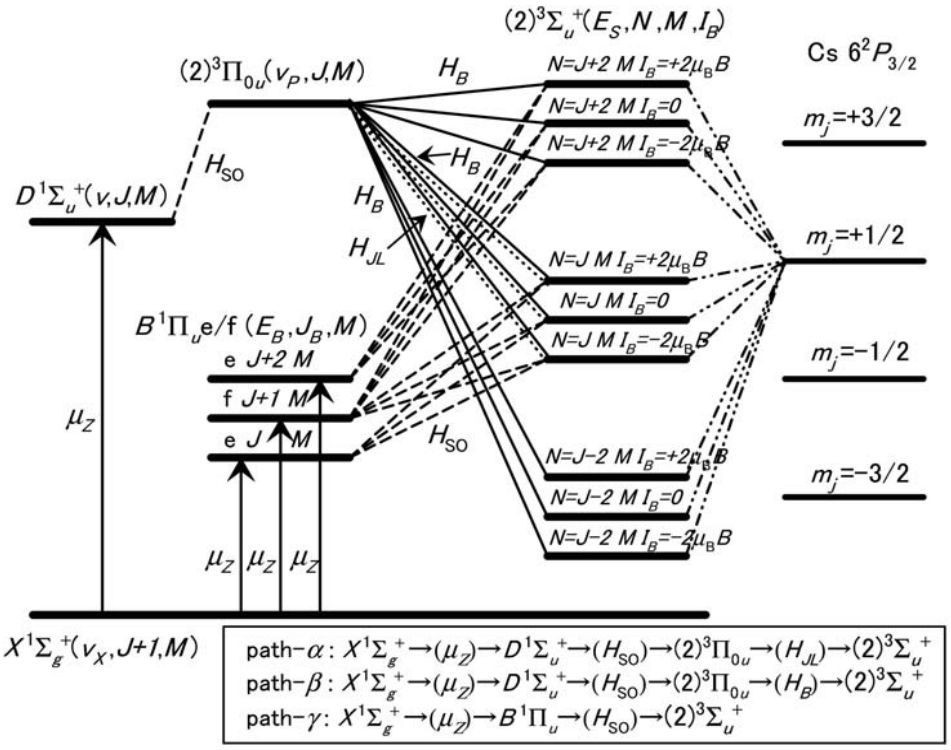

Fig. 5. Levels related to the excitation and the dissociation and couplings between them. Levels coupled by the spin-orbit coupling H_{SO} are connected by broken lines, those by the Zeeman coupling H_B are by straight lines, and those by the L-uncoupling H_{JL} are by dotted lines. Symbol e and f represents levels with parity $+(-)^J$ and $-(-)^J$, respectively.

body-fixed coordinates with the z-axis along the internuclear axis of the Cs_2 molecules where $\boldsymbol{L}$ is an electronic orbital angular momentum [29]. The basis functions of these levels are summarized in Appendix.

When the magnetic field is applied, the three $(2)^3\Sigma_u^+(E_S,N=J,J,M)$ and $(2)^3\Sigma_u^+(E_S,N=J,J\pm1,M)$ continua are mixed, and split into three components $(2)^3\Sigma_u^+(E_S,N=J,M,I_B=0)$ and $(2)^3\Sigma_u^+(E_S,N=J,M,I_B=\pm2\mu_{\mathrm{B}}B)$, [29,30], where I_B indicates three components by their energy shifts in the field. The Zeeman coupling $H_B=-\boldsymbol{m}\cdot\boldsymbol{B}$ couples the $(2)^3\Pi_{0u}\mathrm{e}(v_P,J,M)$ level with $(2)^3\Sigma_u^+(E_S,N,M,I_B)$ continua, which also induces the predissociation (path-β), where $\boldsymbol{m}$ is the magnetic moment of the Cs_2 molecule given by $\boldsymbol{m}=-\mu_{\mathrm{B}}(\boldsymbol{L}+2\boldsymbol{S})/\hbar$.

Kimura et al. have pointed out that a direct excitation from the ground $\mathrm{X}\,^1\Sigma_g^+$ state to the $(2)^3\Sigma_u^+$ state is allowed by spin-orbit coupling of the $(2)^3\Sigma_u^+$ state with the $\mathrm{B}\,^1\Pi_u$ state, and it causes the dissociation into Cs $6p\,^2\mathrm{P}_{3/2}$+ Cs $6s\,^2\mathrm{S}_{1/2}$ atomic fragments (path-γ) [25]. Note that for all these couplings, the selection rule $\Delta M=0$ holds.

In the first order approximation, the probability of the dissociation light producing Cs $6p\,^2\mathrm{P}_{3/2,m_j}$ atomic fragments following to the $\mathrm{X}\,^1\Sigma_g^+(v_{\mathrm{X}},J+1,M)-\mathrm{D}\,^1\Sigma_u^+(v,J,M)$ transition, for which magnetic sublevels (M) are degenerated, is proportional to,

see equation (4) below

where all $2J+1$ degenerated transitions are assumed to be equally stimulated by the dissociation light, and the μ_Z is the transition dipole moment parallel to the field, E_B is the energy, J_B is the quantum number associated with the total angular momentum of the $\mathrm{B}\,^1\Pi_u$ state, Symbol e and f represents levels with parity $+(-)^J$ and $-(-)^J$ of the $\mathrm{B}\,^1\Pi_u$ state, respectively. Symbol ΔE_{DP}, ΔE_{PS}, ΔE_{BS} are the energy differences between $\mathrm{D}^1\Sigma_u^+(v,J,M)$ and $(2)^3\Pi_{0u}\mathrm{e}(v_P,J,M)$,

$$
\begin{aligned}
F_{m_j}=F_0\sum_M\sum_{N,I_B}\Bigg|&\langle \mathrm{X}\,^1\Sigma_g^+(v_X,J+1,M)|\mu_Z|\mathrm{D}\,^1\Sigma_u^+(v,J,M)\rangle\frac{\langle \mathrm{D}\,^1\Sigma_u^+(v,J,M)|H_{\mathrm{SO}}|(2)^3\Pi_{0u}\mathrm{e}(v_P,J,M)\rangle}{\Delta E_{DP}}\\
&\times\int\Big(\frac{\langle(2)^3\Pi_{0u}\mathrm{e}(v_P,J,M)|H_{JL}|(2)^3\Sigma_u^+(E_S,N,M,I_B)\rangle}{\Delta E_{PS}}+\frac{\langle(2)^3\Pi_{0u}\mathrm{e}(v_P,J,M)|H_B|(2)^3\Sigma_u^+(E_S,N,M,I_B)\rangle}{\Delta E_{PS}}\Big)\mathrm{d}E_S\\
&+\sum_{J_B=J}^{J+2}\int\int\langle X\,^1\Sigma_g^+(v_{\mathrm{X}},J+1,M)|\mu_Z|B\,^1\Pi_u\mathrm{e/f}(E_B,J_B,M)\rangle\\
&\times\frac{\langle B\,^1\Pi_u\mathrm{e/f}(E_B,J_{\mathrm{B}},M)|H_{\mathrm{SO}}|(2)^3\Sigma_u^+(E_S,N,M,I_B)\rangle}{\Delta E_{BS}}\mathrm{d}E_B\mathrm{d}E_S\Bigg|^2Q((2)^3\Sigma_u^+(E_S,N,M,I_B),6p\,^2P_{3/2,m_j}),
\end{aligned}
\tag{4}
$$

Table 2. J-dependent coefficients $T^{(|m_j|)}$ with their numerical values for $J = 54$, in units of F_0.

$T^{(\lvert m_j\rvert)}$	analytic	numerical
$T_\alpha^{(3/2)}$	$\frac{J(J+1)(3J^2+8J+6)}{15(2J+1)(2J+3)}$	150.3
$T_\beta^{(3/2)}$	$\frac{416J^8+2448J^7+5216J^6+5008J^5+3182J^4+1515J^3-2972J^2-2716J+1358}{210(2J-1)^2(2J+1)^3(2J+3)^3}$	0.007863
$T_\gamma^{(3/2)}$	$\frac{2(7J^2+21J+31)}{15(2J+1)(2J+3)}$	0.2377
$T_{\alpha\beta}^{(3/2)}$	$+\frac{J^2(J+1)}{15(2J-1)(2J+1)(2J+3)}$	+0.008258
$T_{\beta\gamma}^{(3/2)}$	$+\frac{2(36J^5+132J^4-67J^3-720J^2-470J+402)}{105(2J-1)(2J+1)^2(2J+3)^2}$	+0.02145
$T_{\gamma\alpha}^{(3/2)}$	$-\frac{2J(J+1)(3J+4)}{15(2J+1)(2J+3)}$	−5.433
$T_\alpha^{(1/2)}$	$\frac{J(J+1)(11J^2+26J+12)}{45(2J+1)(2J+3)}$	182.6
$T_\beta^{(1/2)}$	$\frac{1440J^8+7888J^7+15040J^6+10288J^5-1874J^4-6617J^3-2522J^2+1806J+336}{630(2J-1)^2(2J+1)^3(2J+3)^3}$	0.009006
$T_\gamma^{(1/2)}$	$\frac{2(19J^2+57J+27)}{45(2J+1)(2J+3)}$	0.2149
$T_{\alpha\beta}^{(1/2)}$	$-\frac{J(J+1)(J+2)}{45(2J-1)(2J+1)(2J+3)}$	−0.002854
$T_{\beta\gamma}^{(1/2)}$	$+\frac{2(J+2)(44J^4+148J^3+319J^2+722J-438)}{315(2J-1)(2J+1)^2(2J+3)^2}$	+0.009043
$T_{\gamma\alpha}^{(1/2)}$	$-\frac{2J(J+1)(11J+18)}{45(2J+1)(2J+3)}$	−6.676

between $(2)^3\Pi_{0u}\mathrm{e}(v_P, J, M)$ and $(2)^3\Sigma_u^+(E_S, N, M, I_B)$, between $(2)^3\Sigma_u^+(E_S, N, M, I_B)$ and $\mathrm{B}\,^1\Pi_u\mathrm{e/f}(E_B, J_B, M)$, respectively. Here, F_0 is a constant for normalizing F_{m_j} by $\sum_{m_j} F_{m_j} = 1$. This normalization leads the F_{m_j} to be physically equivalent to σ_{m_j} determined from the experiment. The matrix elements of μ_Z, H_{SO}, and H_{JL} are given in reference [29]. Term $Q((2)^3\Sigma_u^+(E_S, N, M, I_B), 6p\,^2\mathrm{P}_{3/2,m_j})$ is a probability of producing Cs $6p\,^2\mathrm{P}_{3/2,m_j}$ atomic fragments by the dissociation from the $(2)^3\Sigma_u^+(E_S, N, M, I_B)$ continuum of the molecules. Singer et al. presented a formula on the correlation between the molecular basis functions and the atomic basis functions for estimating the photodissociation rate from the diatomic molecules [31]. By using the formula, the $Q((2)^3\Sigma_u^+(E_S, N, M, I_B), 6p\,^2\mathrm{P}_{3/2,m_j})$ have been calculated and are listed in Table 1 of reference [30]. Note that in the term $Q((2)^3\Sigma_u^+(E_S, N, M, I_B), 6p\,^2\mathrm{P}_{3/2,m_j})$, the averaging all over the angle between the internuclear axis and the magnetic field direction is included, corresponding to the angle-averaged populations σ_{m_j} determined by the experiment.

Equation (4) shows that the probability of dissociating into each $6p\,^2\mathrm{P}_{3/2,m_j}$ magnetic sublevel is represented by the square of the superposition of the three amplitudes corresponding to each excitation and dissociation path: path-α, path-β and path-γ. Therefore, finally, F_{m_j} are summarized to be a quadratic form of new variables α, β, and γ,

$$F_{\pm 3/2} = T_\alpha^{(3/2)}\alpha^2 + T_\beta^{(3/2)}\beta^2 + T_\gamma^{(3/2)}\gamma^2 \pm T_{\alpha\beta}^{(3/2)}\alpha\beta \pm T_{\beta\gamma}^{(3/2)}\beta\gamma + T_{\gamma\alpha}^{(3/2)}\gamma\alpha, \quad (5)$$

$$F_{\pm 1/2} = T_\alpha^{(1/2)}\alpha^2 + T_\beta^{(1/2)}\beta^2 + T_\gamma^{(1/2)}\gamma^2 \pm T_{\alpha\beta}^{(1/2)}\alpha\beta \pm T_{\beta\gamma}^{(1/2)}\beta\gamma + T_{\gamma\alpha}^{(1/2)}\gamma\alpha, \quad (6)$$

where $T^{(|m_j|)}$'s are J-dependent coefficients which are listed in Table 2 with their numerical values for $J = 54$. Variables α, β, γ are J-independent parts of the amplitude for each path (path-α, path-β, path-γ),

$$\alpha = \mu_\parallel \langle v_X|v\rangle\langle D\,^1\Sigma_u^+|H_{\mathrm{SO}}|(2)^3\Pi_{0u}\rangle \times \langle v|v_P\rangle\langle 1|L_+|0^+\rangle\langle v_P|B_{\mathrm{R}}|E_S\rangle/(\Delta E_{DP}\Delta E_{PS}), \quad (7)$$

$$\beta = \mu_\parallel \langle v_X|v\rangle\langle D\,^1\Sigma_u^+|H_{\mathrm{SO}}|(2)^3\Pi_{0u}\rangle \times \langle v|v_P\rangle\langle 1|L_+|0^+\rangle\langle v_P|E_S\rangle\mu_{\mathrm{B}}B/(\Delta E_{DP}\Delta E_{PS}), \quad (8)$$

$$\gamma = \mu_\perp \langle v_X|E_S\rangle\langle B\,^1\Pi_u|H_{\mathrm{SO}}|(2)^3\Sigma_u^+\rangle/\Delta E_{BS}, \quad (9)$$

$$O_0 = \frac{1}{\sqrt{15}} \frac{(3T^{(3/2)}_{\alpha\beta} + T^{(1/2)}_{\alpha\beta})\alpha\beta + (3T^{(3/2)}_{\beta\gamma} + T^{(1/2)}_{\beta\gamma})\beta\gamma}{(T^{(3/2)}_{\alpha} + T^{(1/2)}_{\alpha})\alpha^2 + (T^{(3/2)}_{\beta} + T^{(1/2)}_{\beta})\beta^2 + (T^{(3/2)}_{\gamma} + T^{(1/2)}_{\gamma})\gamma^2 + (T^{(3/2)}_{\gamma\alpha} + T^{(1/2)}_{\gamma\alpha})\gamma\alpha} \tag{11}$$

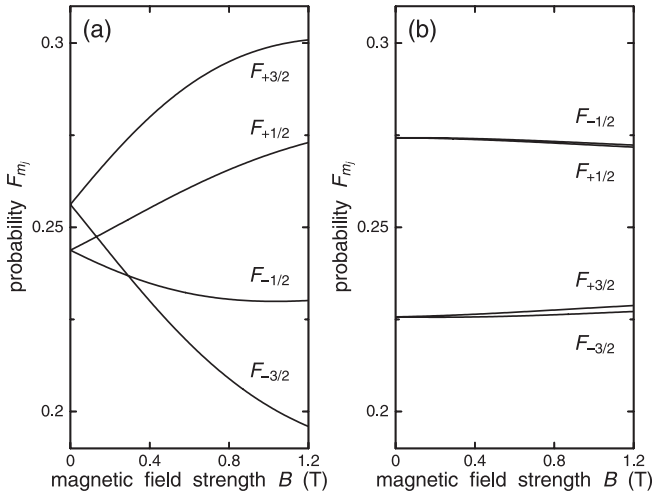

Fig. 6. (a) Calculated probability F_{m_j} producing $6p\,^2\mathrm{P}_{3/2,m_j}$ atoms by the dissociation. (b) Similar when the amplitude from the direct excitation γ is set to be zero.

where $\mu_\parallel$ is the transition dipole moment parallel to the internuclear axis associated with the $\mathrm{X}\,^1\Sigma_g^+ - \mathrm{D}\,^1\Sigma_u^+$ transition, and $\mu_\perp$ is that perpendicular to it with the $\mathrm{X}\,^1\Sigma_g^+ - \mathrm{B}\,^1\Pi_u$ transition. The matrix elements $\langle \mathrm{D}\,^1\Sigma_u^+|H_{\mathrm{SO}}|(2)^3\Pi_{0u}\rangle$ and $\langle \mathrm{B}\,^1\Pi_u|H_{\mathrm{SO}}|(2)^3\Sigma_u^+\rangle$ are electronic parts of the spin-orbit coupling operator. From these equations, it is understood that the dissociated atoms are produced through three coherent excitation and dissociation paths. The terms $T^{(|m_j|)}_{\alpha}\alpha^2$, $T^{(|m_j|)}_{\beta}\beta^2$, and $T^{(|m_j|)}_{\gamma}\gamma^2$ represent the probability, if only each single path is present, and the terms $T^{(|m_j|)}_{\alpha\beta}\alpha\beta$, $T^{(|m_j|)}_{\beta\gamma}\beta\gamma$, and $T^{(|m_j|)}_{\gamma\alpha}\gamma\alpha$ represent the interference between the two paths.

The ratio β/α is given by $\mu_{\mathrm{B}}B\langle v_P|E_S\rangle/\langle v_P|B_{\mathrm{R}}|E_S\rangle$. It is approximated to be $\mu_{\mathrm{B}}B/\overline{B_{\mathrm{R}}}$ [32]. Here, $\overline{B_{\mathrm{R}}}$ is the rotational constant at the internuclear distance 6.5 Å, where the potential energy curve of the $(2)^3\Pi_{0u}$ state crosses with that of the $(2)^3\Sigma_u^+$ state. Then, β/α is given by,

$$\beta/\alpha = 77.8B, \tag{10}$$

where B is in units of T. Since an accurate evaluation of γ/α is difficult, it has been evaluated to be 22.5 by fitting the calculated F_{m_j} to the observed σ_{m_j}.

Figure 6a shows the dependence of the calculated F_{m_j} on the field strength B. The non-zero orientation O_0 is reproduced. Although the quantitative agreement between the calculated F_{m_j} and observed σ_{m_j} is not within the experimental uncertainty, the calculated F_{m_j} are in agreement with the observed ones in the order $F_{+3/2} > F_{+1/2} > F_{-1/2} > F_{-3/2}$ and in the increase of O_0 with the increase of the field strength. By neglecting the contribution from the direct $\mathrm{X}\,^1\Sigma_g^+ - (2)^3\Sigma_u^+$ excitation, i.e. by taking $\gamma = 0$, the probability F_{m_j} have been also calculated. Figure 6b shows the results. In this case $F_{+|m_j|}$ is nearly equal to $F_{-|m_j|}$, i.e. $O_0 \simeq 0$. This result contradicts with the observed one. From this, it is understood that the direct excitation (path-γ) plays an important role for the generation of the orientation O_0 in the ensemble of the atomic fragments.

From equations (3, 5, 6), the orientation O_0 is represented by,

see equation (11) above.

It is understood that the orientation O_0 is induced only when the external magnetic field B is applied, from the fact that β depends on the field strength and other variables α and γ are independent of it. This is reasonable because the direction of the magnetic field reverses under the reflection in the plane perpendicular to the field (space-fixed XY-plane), and therefore the orientation O_0 proportional to $\langle j_Z\rangle$ is allowed. Equation (11) also shows that for small B (thus small β) the orientation O_0 increases as the field strength increases which is in agreement with the experimental result.

Figure 7 shows the contributions to the calculated F_{m_j} for $B = 0.38$ T from each terms $T^{(m_j)}_{\alpha}\alpha^2$, $T^{(m_j)}_{\beta}\beta^2$, $T^{(m_j)}_{\gamma}\gamma^2$, $\pm T^{(m_j)}_{\alpha\beta}\alpha\beta$, $\pm T^{(m_j)}_{\beta\gamma}\beta\gamma$, and $T^{(m_j)}_{\gamma\alpha}\gamma\alpha$. The contributions from the terms $T^{(m_j)}_{\alpha}\alpha^2$ and $T^{(m_j)}_{\gamma}\gamma^2$ are comparable but the one from the $T^{(m_j)}_{\beta}\beta^2$ is small. Among the interference terms, the contribution from term $T^{(m_j)}_{\gamma\alpha}\gamma\alpha$ is dominant but it generates no orientation O_0. Terms $T^{(m_j)}_{\alpha\beta}\alpha\beta$, $T^{(m_j)}_{\beta\gamma}\beta\gamma$ generates the orientation O_0. From the relation $|T^{(m_j)}_{\alpha\beta}\alpha\beta| \ll |T^{(m_j)}_{\beta\gamma}\beta\gamma|$, the orientation O_0 is induced dominantly by the term $T^{(m_j)}_{\beta\gamma}\beta\gamma$ which represents the interference between path-β and path-γ i.e. the coherent superposition of parallel and perpendicular excitation transitions. Here, the reason why $\gamma = 0$ has led almost zero orientation O_0 (Fig. 6b) can be understood well. Small orientation is induced from the term $T^{(m_j)}_{\alpha\beta}\alpha\beta$, which appeared clearly in Figure 6b. The term $T^{(m_j)}_{\alpha\beta}\alpha\beta$ is the coherent superposition of two parallel transitions. It is demonstrated that the orientation O_0 can arise even by the superposition of only parallel transitions when the magnetic field is applied.

In the novel model proposed by Rakitzis et al., a number of electronic states which approach to the same dissociation limit are considered. The phase of the vibrational wavefunction of each states differs at a long internuclear distance, and the interference arisen from the phase differences generates the orientation of the atomic fragments [16,33]. In the present case, however, it is understood from equations (5–9) and Table 2 that the interference arises from the rotational part including the

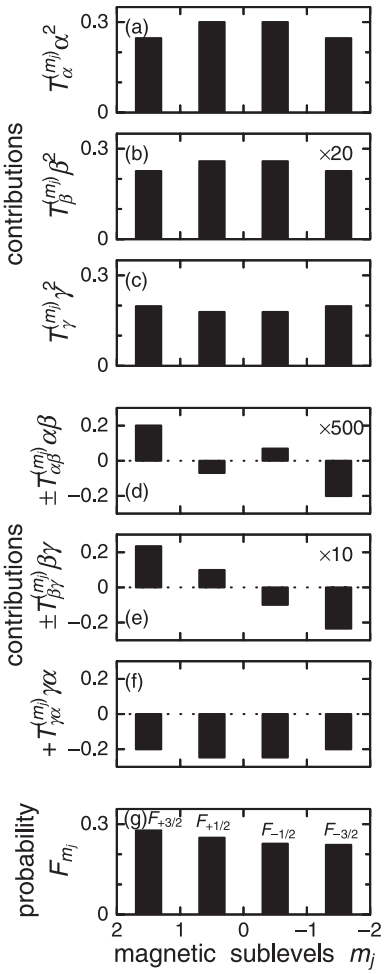

Fig. 7. Contributions from each six term in F_{m_j} for the field strength 0.38 T. (a) Contribution from the term $T_\alpha^{(m_j)}\alpha^2$. (b) $T_\beta^{(m_j)}\beta^2$. (c) $T_\gamma^{(m_j)}\gamma^2$. (d) $\pm T_{\alpha\beta}^{(m_j)}\alpha\beta$. (e) $\pm T_{\beta\gamma}^{(m_j)}\beta\gamma$, (f) $+T_{\gamma\alpha}^{(m_j)}\gamma\alpha$. (g) The sum of the six terms shown in (a) $\sim$ (f), which is identical to F_{m_j}.

electronic and rotational couplings. This is the essential difference between the present result and the one reported by Rakitzis et al. In the present formula, the phases of the vibrational wavefunctions are included in the overlap integrals, $\langle v_X|v\rangle$, $\langle v|v_P\rangle$, $\langle v_P|E_S\rangle$ and $\langle v_X|E_S\rangle$ in α, β and γ (Eqs. (7–9)). The phase differences of the the overlap integrals $\langle v_P|E_S\rangle$ and $\langle v_X|E_S\rangle$ among the three triplet components of the $(2)^3\Sigma_u^+$ states which are mixed in the magnetic field and approach to the same dissociation limit, might be important. However, in the present calculation, $\langle v_P|E_S\rangle$ and $\langle v_X|E_S\rangle$ are approximated to be identical for three triplet components, because the difference of the overlap integrals $\langle v_P|E_S\rangle$ among the three triplet components have been considered *phenomenologically* in the previous report of the author's group [24], but the effect for the generation of the orientation of atomic fragments have been too small.

It is summarized that in the present case the orientation in the ensemble of the atomic fragments is induced by the magnetic field through the interference of the rotational states between the different excitation and dissociation paths and among the three kinds of the interference, the contribution from the one between the field-induced predissociation (path-β) and the direct excitation (path-γ) is dominant.

It is understood from equation (11) and Table 2, that the sign of the orientation O_0 is determined by the (relative) signs of the α, β, and γ. The β/α is estimated to be positive by equation (10), while the sign of γ/α is determined by the signs of the overlap integrals $\langle v_X|E_S\rangle$, $\langle v_X|v\rangle$, $\langle v|v_P\rangle$, and $\langle v_P|E_S\rangle$. Therefore, a negative orientation O_0 of the Cs $6p\,^2\mathrm{P}_{3/2}$ atomic fragments would be possible, if they are dissociated from the other vibrational (v) levels of the $\mathrm{D}\,^1\Sigma_u^+$ state.

From the conservation of the angular momentum, the following two cases are possible after the dissociation, (i) the ensemble of the Cs $6s\,^2\mathrm{S}_{1/2}$ atomic fragments simultaneously produced with the Cs $6p\,^2\mathrm{P}_{3/2}$ fragments, is negatively oriented, $O_0 < 0$, and the net angular momentum of the ensemble of Cs $6p\,^2\mathrm{P}_{3/2}$+ Cs $6s\,^2\mathrm{S}_{1/2}$ fragments is conserved to be zero, or (ii) the net angular momentum of the ensemble containing Cs $6p\,^2\mathrm{P}_{3/2}$+ Cs $6s\,^2\mathrm{S}_{1/2}$ fragments and Cs_2 molecules in the ground $\mathrm{X}\,^1\Sigma_g^+$ state, is zero. These two cases can be distinguished by detecting Cs $6s\,^2\mathrm{S}_{1/2}$ fragments by the similar manner as the present experiment. However, since the molecular beam in the present set-up, contains also Cs atoms in their ground $6s\,^2\mathrm{S}_{1/2}$ level with the Cs_2 molecules in their ground $\mathrm{X}\,^1\Sigma_g^+$ state, the detection of the Cs $6s\,^2\mathrm{S}_{1/2}$ fragments is difficult.

As Siebbeles et al. has pointed out, the orientation O_0 of the ensemble of the dissociated fragments depends on the angle between the direction of the fragmentation (internuclear axis) and the field direction which is parallel to the polarization direction of the dissociation light [7]. However, since in the present experiment, only the angle-averaged populations σ_{m_j}, and thus the angle-averaged orientation O_0, of the Cs $6p\,^2\mathrm{P}_{3/2}$ atomic fragments are determined, the dissociation probability F_{m_j} averaged all over the direction of the internuclear axis (dissociation direction) are calculated and compared with the experimental results.

In the present calculation, all the states are represented by the basis functions on Hund's coupling case (a), but it is known that at larger internuclear distance, the states become to be well represented by coupling case (c) [32]. If the interferential interactions at the long-range internuclear distance well-described by coupling case (c), which have been neglected in the present are considered, the discrepancy between the populations σ_{m_j} (experiment) and the probability F_{m_J} (calculation) might become smaller. However, it is clear from the field dependence of the observed populations σ_{m_j} which tend to 0.25 in the limit of $B = 0$ shown in Figure 4, that the magnetic field plays an important role for the generation of the orientation O_0, even in the case of the interferential long-range interactions.

In summary, in the magnetic field, Cs_2 molecules were excited from the ground $\mathrm{X}\,^1\Sigma_g^+$ state through the M-degenerated $\mathrm{X}\,^1\Sigma_g^+(v_X = 0,\ J_X = 55) - \mathrm{D}\,^1\Sigma_u^+(v = 46,\ J = 54)$ transition by the laser light linearly polarized parallel to the field. The populations of the $6p\,^2\mathrm{P}_{3/2,m_j}$ magnetic sublevels of the dissociated Cs atomic fragments were determined from the relative strengths of the $6p\,^2\mathrm{P}_{3/2,m_j} - 6d\,^2\mathrm{D}_{3/2,m'_j}$ transitions induced by the probe laser light. Non-zero orientation O_0 was found in the ensemble of dissociated Cs $6p\,^2\mathrm{P}_{3/2}$ atomic fragments, though the parent Cs_2 molecules were excited by linearly polarized light. The orientation O_0 increased as the magnetic field strength increased. The non-zero orientation O_0 and its increase following to the increase of the field strength were explained to be induced through the interference in the excitation and dissociation paths in the presence of an external magnetic field.

The author is grateful to Professor Hajime Kato for his many suggestions and the direction. I wish to thank Professor Masaaki Baba, Professor Shunji Kasahara and Rika Takahashi for their assistance on the experiment.

Appendix: Basis functions

Basis function using the Born-Oppenheimer approximation is defined by,

$$|\Lambda'\rangle|S'\Sigma'\rangle|v'\rangle|J'\Omega'M'\rangle, \tag{A.1}$$

where Λ' denotes the quantum number associated with the projection of the orbital angular momentum $\boldsymbol{L'}$ of the electron on the internuclear axis, S' and Σ' denote the quantum numbers associated with the spin angular momentum $\boldsymbol{S'}$ of the electron and with its projection on the internuclear axis, v' the vibrational quantum number, (E' is the energy of the continuum excluding the rotational energy), J', Ω', M' denote the quantum numbers associated with the total angular momentum $\boldsymbol{J'}$ of the molecule, with its projection along the internuclear axis, and with its projection along the space-fixed Z-axis, respectively.

Basis functions represent the electronic, vibrational and rotational state are,

$$\mathrm{D}, X^1\Sigma_u^+(v', J', M') : |0^+\rangle|00\rangle|v'\rangle|J'0M'\rangle, \tag{A.2}$$

$$\mathrm{B}^1\Pi_u\mathrm{e/f}(E', J', M') : \left[|+1\rangle|00\rangle|E'\rangle|J'+1M'\rangle \pm |-1\rangle|00\rangle|E'\rangle|J'-1M'\rangle\right]/\sqrt{2}, \tag{A.3}$$

$$(2)^3\Pi_{0u}\mathrm{e}(v', J', M') : \left[|+1\rangle|1-1\rangle|v'\rangle|J'0M'\rangle - |-1\rangle|1+1\rangle|v'\rangle|J'0M'\rangle\right]/\sqrt{2}, \tag{A.4}$$

$$\begin{aligned}(2)^3\Sigma_u^+(E', N'=J'+1, J', M') : {}& \sqrt{J'/2(2J'+1)}|0^+\rangle|1+1\rangle|E'\rangle|J'+1M'\rangle - \sqrt{(J'+1)/(2J'+1)}|0^+\rangle|10\rangle|E'\rangle|J'0M'\rangle \\ & + \sqrt{J'/2(2J'+1)}|0^+\rangle|1-1\rangle|E'\rangle|J'-1M'\rangle,\end{aligned} \tag{A.5}$$

$$(2)^3\Sigma_u^+(E', N'=J', J', M') : (1/\sqrt{2})|0^+\rangle|1+1\rangle|E'\rangle|J'+1M'\rangle - (1/\sqrt{2})|0^+\rangle|1-1\rangle|E'\rangle|J'-1M'\rangle, \tag{A.6}$$

$$\begin{aligned}(c)^3\Sigma_u^+(E', N'=J'-1, J', M') : {}& \sqrt{(J'+1)/2(2J'+1)}|0^+\rangle|1+1\rangle|E'\rangle|J'+1M'\rangle \\ & + \sqrt{J'/(2J'+1)}|0^+\rangle|10\rangle|E'\rangle|J'0M'\rangle + \sqrt{(J'+1)/2(2J'+1)}|0^+\rangle|1-1\rangle|E'\rangle|J'-1M'\rangle,\end{aligned} \tag{A.7}$$

where, e and f represent levels with parity $+(-)^J$ and $-(-)^J$, respectively, and in equation (A.3) the 'e' level is represented by the state vector with plus sign and 'f' minus sign. The symbol N' denotes the quantum number associated with $\boldsymbol{J'} - \boldsymbol{S'}$.

Three continua $(2)^3\Sigma_u^+(E', N' = J', J'+1, M')$, $(2)^3\Sigma_u^+(E', N' = J', J', M')$, $(2)^3\Sigma_u^+(E', N' = J', J'-1, M')$ are degenerated and they are mixed in the magnetic field,

$$\begin{aligned}(2)^3\Sigma_u^+(E', N'=J', M', I_B = +2\mu_\mathrm{B}B) : {}& + \sqrt{(J'+M')(J'+M'+1)/2(J'+1)(2J'+1)}|c^3\Sigma_u^+(E', N'=J', J'+1, M')\rangle \\ & + \sqrt{(J'+M')(J'-M'+1)/2J'(J'+1)}|c^3\Sigma_u^+(E', N'=J', J', M')\rangle \\ & + \sqrt{(J'-M')(J'-M'+1)/2J'(2J'+1)}|c^3\Sigma_u^+(E', N'=J', J'-1, M')\rangle,\end{aligned} \tag{A.8}$$

$$\begin{aligned}(2)^3\Sigma_u^+(E', N'=J', M', I_B = 0) : {}& - \sqrt{(J'+M'+1)(J'-M'+1)/(J'+1)(2J'+1)}|(2)^3\Sigma_u^+(E', N'=J', J'+1, M'\rangle \\ & + \left(M'/\sqrt{J'(J'+1)}\right)|(2)^3\Sigma_u^+(E', N'=J', J', M')\rangle \\ & + \sqrt{(J'+M')(J'-M')/J'(2J'+1)}|(2)^3\Sigma_u^+(E', N'=J', J'-1, M'\rangle,\end{aligned} \tag{A.9}$$

$$\begin{aligned}(2)^3\Sigma_u^+(E', N'=J', M', I_B = -2\mu_\mathrm{B}B) : {}& - \sqrt{(J'-M'+1)(J'-M')/2(J'+1)(2J'+1)}|(2)^3\Sigma_u^+(E', N'=J', J'+1, M')\rangle \\ & + \sqrt{(J'-M')(J'+M'+1)/2J'(J'+1)}|(2)^3\Sigma_u^+(E', N'=J', J', M')\rangle \\ & - \sqrt{(J'+M')(J'+M'+1)/2J'(2J'+1)}|(2)^3\Sigma_u^+(E', N'=J', J'-1, M')\rangle,\end{aligned} \tag{A.10}$$

where I_B indicates three components by their energy shifts in the field and μ_B is the Bohr magneton.

References

1. C.H. Greene, R.N. Zare, Ann. Rev. Phys. Chem. **33**, 119 (1982)
2. S.J. Singer, K.F. Freed, Y.B. Band, Adv. Chem. Phys. **61**, 1 (1985)
3. U. Fano, J.H. Macek, Rev. Mod. Phys. **45**, 553 (1973)
4. K. Blum, *Density Matrix Theory and Applications* (Plenum, New York, 1981)
5. R.N. Zare, *Angular Momentum* (John Wiley, New York, 1988)
6. R.N. Dixon, J. Chem. Phys. **85**, 1866 (1986)
7. L.D.A. Siebbeles, M. Glass-Maujean, O.S. Vasyutinskii, J.A. Beswick, O. Roncero, J. Chem. Phys. **100**, 3610 (1994)
8. M. Brouard, P. O'Keeffe, D.M. Joseph, D. Minayev, Phys. Rev. Lett. **86**, 2249 (2001)
9. M.L. Costen, S.W. North, G.E. Hall, J. Chem. Phys. **111**, 6735 (1999)
10. A.J. Alexander, Phys. Rev. A **66**, 060702 (2002)
11. T.P. Rakitzis, P.C. Samartzis, T.N. Kitsopoulos, Phys. Rev. Lett. **87**, 123001 (2001)
12. S.M. Dylewski, J.D. Geiser, P.L. Houston, J. Chem. Phys. **115**, 7460 (2001)
13. O.S. Vasyutinskii, JETP Lett. **31**, 428 (1980)
14. D.V. Kupriyanov, B.V. Picheyev, O.S. Vasyutinskii, J. Phys. B **26**, L803 (1993)
15. A.G. Evseev, D.V. Kupriyanov, B.V. Picheyev, B.N. Sevastianov, O.S. Vasyutinskii, Chem. Phys. **171**, 45 (1993)
16. T.P. Rakitzis, S.A. Kandel, A.J. Alexander, Z.H. Kim, R.N. Zare, Science **281**, 1346 (1998)
17. S. Kasahara, K. Otsuka, M. Baba, H. Katô, J. Chem. Phys. **109**, 3393 (1998)
18. C. Amiot, W. Demtröder, C.R. Vidal, J. Chem. Phys. **88**, 5265 (1988)
19. U. Diemer, R. Duchowicz, M. Ertel, E. Mehdizadeh, W. Demtröder, Chem. Phys. Lett. **164**, 419 (1989)
20. N. Spies, Ph.D. thesis, Fachbereich Chemie, Universität Kaiserslautern, 1989
21. C.B. Collins, F.W. Lee, J.A. Anderson, P.A. Vicharelli, D. Popescu, I. Popescu, J. Chem. Phys. **74**, 1067 (1981)
22. M. Raab, G. Höning, W. Demtröder, C.R. Vidal, J. Chem. Phys. **76**, 4370 (1982)
23. H. Katô, T. Kobayashi, M. Chosa, T. Nakahori, T. Iida, S. Kasahara, M. Baba, J. Chem. Phys. **94**, 2600 (1991)
24. K. Matsubara, Y. Tajima, M. Baba, J. Kawai, H. Katô, Bull. Chem. Soc. Jpn **69**, 2839 (1996)
25. Y. Kimura, H. Lefebvre-Brion, S. Kasahara, H. Katô, M. Baba, R. Lefebvre, J. Chem. Phys. **113**, 8637 (2000)
26. E. Arimondo, M. Inguscio, P. Violino, Rev. Mod. Phys. **49**, 31 (1977)
27. E.U. Condon, G.H. Shortley, *The Theory of Atomic Spectra* (University Press, Cambridge, 1951)
28. A. Corney, *Atomic and Laser Spectroscopy* (Clarendon, Oxford, 1977)
29. H. Katô, Bull. Chem. Soc. Jpn **66**, 3203 (1993)
30. H. Katô, K. Onomichi, J. Chem. Phys. **82**, 1642 (1985)
31. S.J. Singer, K.F. Freed, Y.B. Band, J. Chem. Phys. **79**, 6060 (1983)
32. H. Lefebvre-Brion, R.W. Field, *Perturbations in the Spectra of Diatomic Molecules* (Academic Press, Orlando, 1986)
33. T.P. Rakitzis, P.C. Samartzis, R.L. Toomes, T.N. Kitsopoulos, A. Brown, G.G. Balint-Kurti, V.S. Vasyutinskii, J.A. Beswick, Science **300**, 1936 (2003)